

A 1.55 μ W Bio-Impedance Measurement System for Implantable Cardiac Pacemakers in 0.18 μ m CMOS

Zamani, Milad; Rezaeiyan, Yasser; Shoaee, Omid; Serdijn, Wouter A.

DOI

[10.1109/TBCAS.2017.2776528](https://doi.org/10.1109/TBCAS.2017.2776528)

Publication date

2018

Document Version

Final published version

Published in

IEEE Transactions on Biomedical Circuits and Systems

Citation (APA)

Zamani, M., Rezaeiyan, Y., Shoaee, O., & Serdijn, W. A. (2018). A 1.55 μ W Bio-Impedance Measurement System for Implantable Cardiac Pacemakers in 0.18 μ m CMOS. *IEEE Transactions on Biomedical Circuits and Systems*, 12(1), 211-221. Article 8248760. <https://doi.org/10.1109/TBCAS.2017.2776528>

Important note

To cite this publication, please use the final published version (if applicable). Please check the document version above.

Copyright

Other than for strictly personal use, it is not permitted to download, forward or distribute the text or part of it, without the consent of the author(s) and/or copyright holder(s), unless the work is under an open content license such as Creative Commons.

Takedown policy

Please contact us and provide details if you believe this document breaches copyrights. We will remove access to the work immediately and investigate your claim.

A 1.55 μW Bio-Impedance Measurement System for Implantable Cardiac Pacemakers in 0.18 μm CMOS

Milad Zamani ¹, Student Member, IEEE, Yasser Rezaeiyan ¹, Omid Shoaee ¹, Member, IEEE, and Wouter A. Serdijn ², Fellow, IEEE

Abstract—This paper presents an implantable bio-impedance measurement system for cardiac pacemakers. The fully integrated system features a low power analog front-end and pulse width modulated output. The bio-impedance readout benefits from voltage to time conversion to achieve a very low power consumption for wirelessly transmitting the data outside the body. The proposed IC is fabricated in a 0.18 μm CMOS process and is capable of measuring the bio-impedance at 2 kHz over a wide dynamic range from 100 Ω to 3.3 k Ω with 1.35 Ω_{rms} accuracy and 1 μA maximum current injection while consuming just 1.55 μA from a 1 V supply.

Index Terms—Analog circuit design, bio-impedance, biosensor, cardiac tissue, CMOS, low power, impedance measurement, instrumentation amplifier, programmable amplifier.

I. INTRODUCTION

IN NORMAL subjects, the heart rate during exercise increases proportionally to oxygen consumption, which is the most accurate measure of human energy expenditure [1], [2]. Bio-impedance measurement provides useful information about physiological processes, such as breathing and heart rate, which are related to the oxygen consumption and tidal volume and in the frequency bands of 0.1–1 Hz and 1–3 Hz, respectively, [3], [4], [15]. The fast change of bio-impedance is mostly related to the beating of the heart and the low change is related to the breathing and respiratory components [5]. Thus, bio-impedance measurement can be effectively used to extract cardiac and respiratory parameters. Rate-adaptive pacemakers use the information of periodical variation of the thoracic bio-impedance to change the rate of heart muscle stimulation [4].

Fig. 1 shows the lead and heart lumped electrical impedance model. The lead resistances of cathode and anode are represented by R_C and R_A , respectively. Taking the electrode areas into account, the cathode and anode capacitances are C_{HC} and

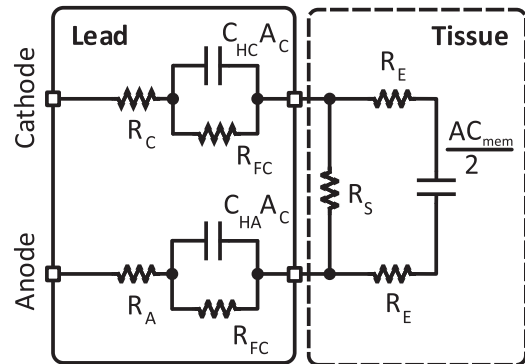


Fig. 1. Lead and heart tissue electrical model [2].

C_{HA} , which are the Helmholtz capacitances multiplied by their respective electrode area, A_c . R_{FC} is the faradaic resistance of the lead [2].

The tissue three-element impedance model consists of R_E , which represents the resistance comprised by the electrolytes, R_S , which designates the shunt resistance through which current is able to pass through non-excitable tissue and blood outside the desired current path, and the cellular membrane specific capacitance, C_{mem} , multiplied by the cathode's area, A , divided by two, which is assumed being proportional to the number of cells directly surrounding the cathode [2].

Conventional bio-impedance measurement systems inject a semi-square current waveform into the tissue and make use of a lock-in amplifier to produce the in-phase and quadrature components of the bio-impedance. The magnitude and phase of the bio-impedance can be extracted from the digital output signal. An analog to digital converter plays a key role in converting the lock-in amplifier output into a digital format with an appropriate number of bits [6]–[14]. The data analysis and wireless transmission of digital signals are normally power hungry functions. As digital process and the radio usually are the main sources of system power consumption, any improvement of the power consumption must center around the proper output data format for a low power consumption wireless transmission and without any digital processing in the implant [10], [20], [21].

In this paper, a novel bio-impedance measurement technique is proposed that benefits from voltage-to-time conversion and enables the transmission of data at very low power consumption. The proposed system consists of two channels for magnitude and phase measurement, the output of which are PWM signals. The

Manuscript received May 27, 2017; revised August 17, 2017 and October 6, 2017; accepted November 15, 2017. Date of publication January 8, 2018; date of current version January 26, 2018. This paper was recommended by Associate Editor B. Gosselin. (Corresponding Author: Omid Shoaee.)

M. Zamani and Y. Rezaeiyan are with the Bio-Integrated Systems Laboratory, School of Electrical and Computer Engineering, University of Tehran, Tehran 12345, Iran (e-mail: miladzamani@ut.ac.ir; yrezaeiyan@ut.ac.ir).

O. Shoaee is with the Nano-Electronic Center of Excellence and the Bio-Integrated Systems Lab, School of Electrical and Computer Engineering, University of Tehran, Tehran 1439957131, Iran (e-mail: oshoaee@ut.ac.ir).

W. A. Serdijn is with the Section Bioelectronics, Faculty of Electrical Engineering, Mathematics and Computer Science, Delft University of Technology, Delft 2628CD, The Netherlands (e-mail: w.a.serdijn@tudelft.nl).

Color versions of one or more of the figures in this paper are available online at <http://ieeexplore.ieee.org>.

Digital Object Identifier 10.1109/TBCAS.2017.2776528

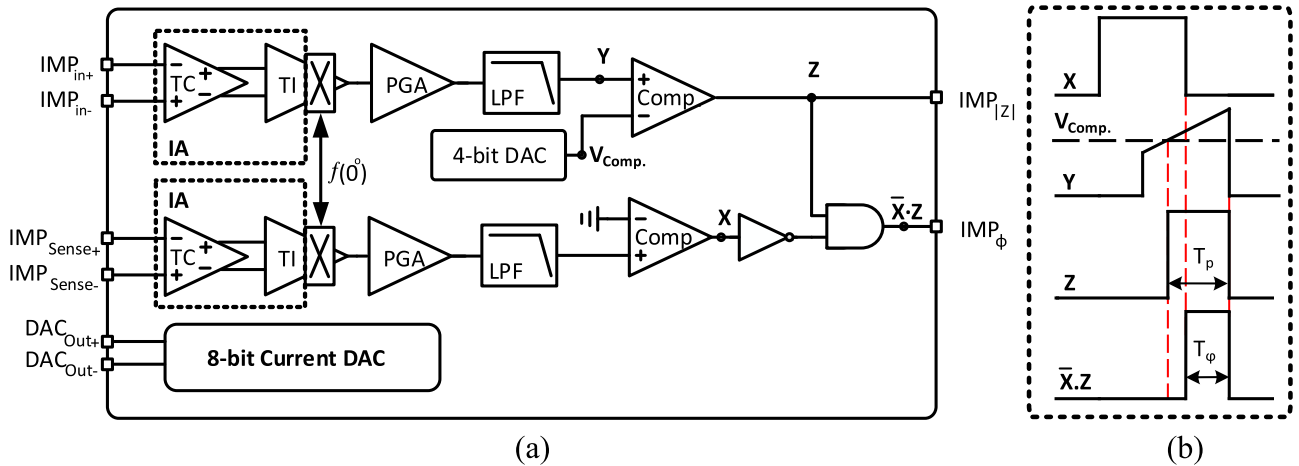


Fig. 2. (a) Architecture of the proposed bio-impedance measurement system. (b) Example of internally generated signals.

magnitude and phase of the bio-impedance are directly related to the pulse width of these PWM signals.

This paper is organized as follows: Section II describes the architecture of the proposed bio-impedance measurement system and detection principle. Section III describes the operation principle and analyzes jitter, linearity and systematic errors. Section IV describes the circuit implementation and requirements. Section V presents the measurement results. Finally, Section VI concludes the paper.

II. ARCHITECTURE AND DETECTION PRINCIPLE

Fig. 2(a) shows the proposed bio-impedance read-out channel which consists of two paths. One path obtains the magnitude of the bio-impedance and another extracts the phase of it. The proposed implementation employs an 8-bit current DAC to inject a 2 kHz semi-ramp current into the heart tissue. The injected current must meet the IEC60601-1 medical standards which defines the maximum amplitude and frequency of the injected current [22]. This standard ensures safe current injection for the bio-impedance measurement with minimum negative effects on the heart tissue.

Fig. 2(b) shows the signals at different nodes of the amplitude and phase channels. The X waveform is the PWM signal from the reference channel, originating from the voltage measured across the reference resistor, which thus is only affected by the phase shift of the readout channel. The Y waveform is the input voltage of the comparator of the amplitude channel which is the down-converted bio-impedance semi-ramp amplitude modulated signal. This signal contains the delay that originates from the readout channel and also the bio-impedance phase. The Z waveform is the output of the amplitude channel with the amplitude data embedded in the pulse width. The last waveform is the difference of the reference signal and the PWM signal of the amplitude channel. The phase data can be reconstructed exactly from its pulse width.

Fig. 3 shows the signals at different nodes of the magnitude and phase channels extracted from a system level simulation in MATLAB. The injected current is a 2 kHz semi-ramp shape current which has positive, zero and negative parts (Fig. 3(a)).

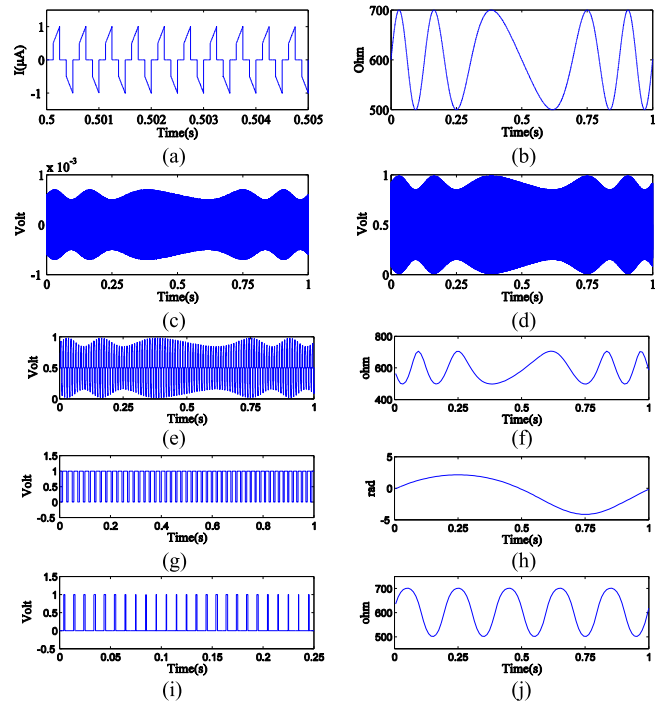


Fig. 3. Bio-impedance system level simulation. a) Semi-ramp DAC output signal. b) Heart tissue bio-impedance with varying magnitude and phase. c) The voltage produced after current injection into the heart tissue. d) The output signal of the mixer. e) The comparator input signal. f) Reconstructed impedance of the tissue impedance. g) The PWM output of the phase channel. h) Reconstructed phase of the heart tissue. i) The PWM output of the magnitude channel. j) Reconstructed magnitude of the heart tissue impedance.

The current injected into the heart tissue is modulated with the bio-impedance magnitude and phase (Fig. 3(c)). Fig. 3(b) shows the heart tissue bio-impedance with magnitude (500Ω to 700Ω) and phase ($-\pi$ radians to π radians) that changes with breathing and other physiological processes. The magnitude readout channel employs an instrumentation amplifier (IA) consisting of a transconductance (TC) and a transimpedance (TI) stage. The IA requires a highly linear (THD below 1%) voltage gain with a low input referred noise (lower than $2 \mu V_{rms}$). The mixer converts the modulated voltage down and produces a 100 Hz baseband

signal (Fig. 3(d)). The magnitude of the heart impedance is in the range of 50 Ω –3.3 k Ω . Higher impedance levels may be caused by leads displacement. The large range of bio-impedance requires a high dynamic range to read the produced voltage. A programmable gain amplifier (PGA) provides 4 different gain settings for 4 different impedance ranges to increase the dynamic range. The intrinsic low-pass filter of the PGA and the subsequent 2-stage switch-capacitor low-pass filter remove any higher frequency components of the mixer output signal. The comparator compares the bio-impedance ramp-modulated signal with a reference voltage. The 4-bit voltage DAC generates the reference voltage for comparison with 8 different voltage levels, which can be set for different impedance ranges and the minimum voltage is set by the largest bit. The output of the comparator is a PWM signal, the pulse-width of which relates directly to the magnitude of the bio-impedance. Reading the pulse width of the PWM signal, the magnitude of the bio-impedance can be reconstructed.

The phase readout channel is the same as the magnitude readout channel with some minor differences. The input signal of the phase readout channel is an ideal voltage generated by the injected current into a reference resistor. Thus, the magnitude and phase of the bio-impedance have no effect on this input voltage signal. The input signal is then amplified, mixed and filtered just like the magnitude readout channel. The comparator compares the signal with zero to define the zero-crossings of the signal. The X signal is the PWM signal from the reference channel and related to the reference resistor, which thus only is affected by the phase shift of the blocks while passing through the phase channel. The Y signal is the input voltage of the comparator of the magnitude channel which is the down-converted version of the bio-impedance semi-ramp magnitude modulated signal. This signal contains the delay that originates from the readout channel and also the bio-impedance phase. The Z signal is the output of the magnitude channel with magnitude data embedded in the pulse width. Comparing the output PWM signal of the phase channel and that of the magnitude channel results in a signal that represents the phase of the bio-impedance. It can be readily noted that the pulse width of the amplitude channel output signal is determined by both the amplitude and the phase of the bio-impedance, as well as the phase shift of the channel itself. The pulse width of the phase channel output signal, used as the reference signal, on the other hand, is only determined by the channel phase shift. From the phase difference of the output signals of these two channels, i.e., $\bar{X}.Z$, the phase of the bio-impedance is extracted. The phase data can be exactly reconstructed from the pulse width of this signal.

The voltage produced after current injection into the heart tissue and the output signal of the mixer are shown in Fig. 3(c) and 3(d), respectively. Fig. 3(e) shows the comparator input signal of the amplitude channel (Y). Fig. 3(f), 3(h) and 3(j) show the reconstructed impedance of the tissue, the reconstructed phase of the heart tissue and the reconstructed magnitude of the heart tissue. Fig. 3(g) and 3(i) show the PWM output of the magnitude channel (Z) and the PWM output of the phase channel ($\bar{X}.Z$), respectively. After injecting the DAC current into the heart tissue the amplitude of the bio-impedance affects

the slope of the voltage across the tissue. The pulse width of the comparator gives the amplitude and the comparison of the ideal phase and the impedance phase gives the phase of the bio-impedance.

III. SYSTEM ANALYSIS

To obtain a deep understanding of the proposed system, we derive closed-form formulae for the magnitude and phase channel output signals. We also conduct a jitter analysis to find the impact of jitter on the reconstructed output signals. The proposed system and the conventional systems use non-sinusoidal signals for injection to decrease the power consumption. Thus, the systematic error must be analyzed at system level.

A. Output PWM Signal of Magnitude and Phase Channels

The signal voltage of the magnitude channel preceding the comparator is the multiplication of the injected current, the magnitude of the bio-impedance of the tissue, the front-end gain and the demodulation clock amplitude. The input semi-ramp signal Fourier series can be calculated as:

$$I(t) = \sum_{n=1}^{\infty} \{a_n \cos(\omega_{osc}nt)\} - \sum_{n=1}^{\infty} \{b_n \sin(\omega_{osc}nt)\} \quad (1)$$

where

$$a_n = \frac{-2a}{\pi^2(2n-1)^2} + \frac{a(-1)^n}{\pi(2n-1)}$$

$$b_n = \frac{2a}{\pi(2n-1)} + \frac{2a(-1)^n}{\pi^2(2n-1)^2} \quad (2)$$

where a is the amplitude of semi-ramp signal and ω_{osc} is the injection current angular frequency.

The signal voltage of the magnitude channel preceding the comparator is

$$V_{in-CompAmp} =$$

$$G_{FE} \sum_{n=1}^{\infty} \left\{ \frac{a_n}{2} |Z_{tissue}(n(\omega_{LF}))| \cos(n\omega_{LF}t + \varphi(n\omega_{LF})) \right\}$$

$$+ G_{FE} \sum_{n=1}^{\infty} \left\{ \frac{b_n}{2} |Z_{tissue}(n(\omega_{LF}))| \sin(n\omega_{LF}t + \varphi(n\omega_{LF})) \right\} \quad (3)$$

where G_{FE} is the channel front-end gain, ϕ is the phase of the bio-impedance and ω_{LF} is the down-converted angular frequency. Z_{tissue} can be represented by the three element (Fig. 1) model as:

$$Z_{tissue}(\omega) = \frac{2R_S R_E (2R_E + R_S) C^2 \omega^2 + R_S}{1 + (2R_E + R_S)^2 C^2 \omega^2}$$

$$- j \frac{R_S^2 C \omega}{1 + (2R_E + R_S)^2 C^2 \omega^2} \quad (4)$$

The magnitude and the phase of the bio-impedance can be written as:

$$|Z(\omega)| = \sqrt{\frac{R_S^2 + 4R_E^2 R_S^2 C^2 \omega^2}{1 + (R_S + 2R_E)^2 C^2 \omega^2}} \quad (5)$$

$$\varphi(\omega) = \tan^{-1} \left(\frac{R_S C \omega}{1 + 2R_E (2R_E + R_S) C^2 \omega^2} \right) \quad (6)$$

where C is $(AC_{\text{mem}})/2$.

(3) can be rewritten as follows:

$$\begin{aligned} V_{in-Comp_{Amp}} &= G_{FE} \sum_{n=1}^{\infty} \left\{ \frac{a_n}{2} |Z_{tissue}(n(\omega_{LF}))| \right. \\ &\times \cos \left[n\omega_{LF} \left(t + \frac{\varphi(n\omega_{LF})}{n\omega_{LF}} \right) \right] \left. \right\} + G_{FE} \sum_{n=1}^{\infty} \\ &\times \left\{ \frac{b_n}{2} |Z_{tissue}(n(\omega_{LF}))| \sin \left[n\omega_{LF} \left(t + \frac{\varphi(n\omega_{LF})}{n\omega_{LF}} \right) \right] \right\} \\ &= G_{FE} \sum_{n=1}^{\infty} \left\{ \frac{a_n}{2} |Z_{tissue}(n(\omega_{LF}))| \cos [n\omega_{LF} (t + \tau_n)] \right\} \\ &+ G_{FE} \sum_{n=1}^{\infty} \left\{ \frac{b_n}{2} |Z_{tissue}(n(\omega_{LF}))| \sin [n\omega_{LF} (t + \tau_n)] \right\}. \end{aligned} \quad (7)$$

Equation (7) shows that the signal voltage of the magnitude channel is the multiplication of the bio-impedance magnitude and the semi-ramp signal with a phase shift equal to the bio-impedance phase. We can suppose that the bio-impedance amplitude is constant in the specific frequency range, since the bio-impedance dependency on frequency is low at low frequencies. Hence, (7) approximates the product of the semi-ramp and the bio-impedance [4], [5].

The comparator compares the bio-impedance semi-ramp modulated signal with a reference voltage. The pulse width of the PWM output signal can be written as

$$T_p(m) = \frac{1}{4f_{LF}} - \frac{\pi V_{ref}}{4\sqrt{2}f_{LF}|Z_{tissue}(m)|I(m)G_{FE}} \quad (8)$$

where m is the m th sample of the current DAC.

The phase channel output signal is the multiplication of the injection current, the reference resistor, the front-end gain and the demodulation clock. The input signal of the phase channel is:

$$\begin{aligned} V_{in-Comp_{\varphi}} &= \sum_{n=1}^{\infty} \left\{ \frac{a_n}{2} R_{sens} \cos(n\omega_{LF} t) \right\} \\ &- \sum_{n=1}^{\infty} \left\{ \frac{b_n}{2} R_{sens} \sin(n\omega_{LF} t) \right\} \end{aligned} \quad (9)$$

where R_{sens} is the reference resistor.

The phase channel provides a similar delay as that of the magnitude channel to compensate for the magnitude read-out phase shift. The comparator produces a pulse depending on the zero-crossing of its input signal. The time difference of the

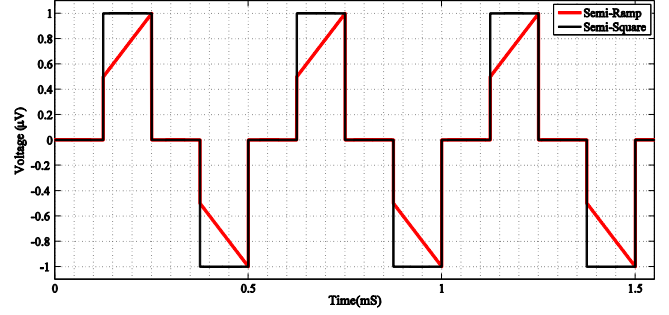


Fig. 4. Semi-ramp and semi-square input signals.

magnitude channel and phase channel pulses is related to the phase of the bio-impedance as:

$$\prod_{\text{phase}} \left(\frac{t}{T_p} \right) = (X \cdot Z) \otimes Z = \bar{X} \cdot Z \quad (10)$$

$$\phi = \frac{2\pi}{T} T_p(t) \quad (11)$$

where X and Z represent the output signals of the phase and magnitude channels, respectively, T_p is the output pulse width and \otimes is a logical XOR.

The PWM output of the magnitude channel and the phase channel can be written as [16]:

$$\begin{aligned} O_{Amp}(t) &= \frac{1}{4} - \frac{\pi V_{comp}}{4\sqrt{2}|Z_{tissue}(m)|I(m)G_{FE}} \\ &+ \frac{2}{\pi} \sum_{k=1}^{\infty} \left\{ \left(\frac{1}{k} \right) \sin \left(\frac{k\pi}{4} - \frac{k\pi^2 V_{comp}}{4\sqrt{2}|Z_{tissue}(m)|I(m)G_{FE}} \right) \right\} \\ &\times \cos(k\omega_{LF} t) \end{aligned} \quad (12)$$

$$O_{\text{phase}}(t) = \frac{\varphi(t)}{2\pi} + \frac{2}{\pi} \sum_{k=1}^{\infty} \left\{ \left(\frac{1}{k} \right) \sin \left(\frac{k\varphi(t)}{2} \right) \cos(k\omega_{LF} t) \right\} \quad (13)$$

where ω_{LF} is down-converted angular frequency, m is the m th sample and V_{comp} is the comparator reference.

Equations (12) and (13) are used for bio-impedance amplitude and phase reconstruction. The accuracy of reconstructed amplitude and phase can be derived from these two equations since they contain non-ideal and non-sinusoidal components. The linearity and systematic error of the system are the deviation of the reconstructed amplitude and phase from the theoretically correct values. The following section describes the analysis of these linearity and systematic errors.

B. Linearity

Most of recent bio-impedance measurement systems use semi-square signals for injection to eliminate the need for power hungry sinusoidal oscillators and analog multipliers [10]. The input signal of such a system is a three-level pulse (semi-square) waveform. See Fig. 4.

As previously explained and shown in Fig. 2 and Fig. 3 the proposed bio-impedance measurement system works as follows:

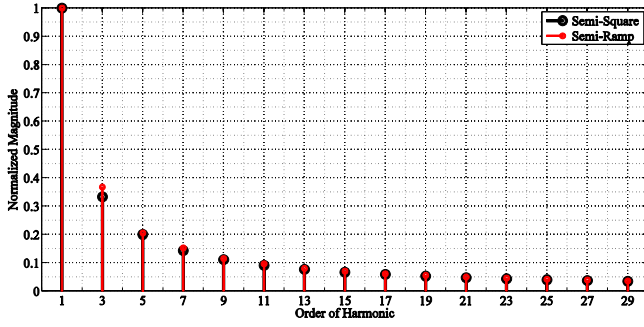


Fig. 5. Magnitude spectrum of the semi-ramp signal and the semi-square signal.

a semi-ramp current is injected into the tissue and by comparing the resultant semi-ramp voltage (which contains both the magnitude and phase information of the tissue bio-impedance) with the injected signal-level (in the magnitude path), and also comparing the output pulse of the so-called magnitude channel with the original (or reference) injected signal that is only phase-shifted by the measurement/phase path both magnitude and phase information of the tissue bio-impedance are extracted.

The output errors come mainly from three sources: 1) the non-sinusoidal injected current, 2) the inaccuracy of the injected current and 3) the systematic error.

1) *Error Due to the Non-Sinusoidal Injected Signal:* The first source of non-linearity is the injected signal. To calculate the impedance at a single frequency a pure sinusoidal source is needed. Using other signals causes an error in the bio-impedance measurement.

The conventional fully bi-directional square wave (semi-square) stimulation current Fourier series can be written as [12]:

$$I_{conv.}(t) = \frac{4}{\pi} \sum_{n=1}^{\infty} \left\{ \left(\frac{1}{(2n-1)} \right) \sin(2n-1)\omega t \right\}. \quad (14)$$

Our system uses a semi-ramp input signal. The input semi-ramp signal (Fig. 5) Fourier series can be calculated as:

$$I(t) = a_0 + \sum_{n=1}^{\infty} \{a_n \cos(\omega t n)\} - \sum_{n=1}^{\infty} \{b_n \sin(\omega t n)\} \quad (15)$$

where

$$\begin{aligned} a_0 &= 0, a = 1, \\ a_{2n-1} &= \frac{-2a}{\pi^2(2n-1)^2} + \frac{a(-1)^n}{\pi(2n-1)}, \\ b_{2n-1} &= \frac{2a}{\pi(2n-1)} + \frac{2a(-1)^n}{\pi^2(2n-1)^2}. \end{aligned}$$

2) *Error Due to the Inaccuracy of the Injected Current:* The accuracy of injected signal is another source of error. Any difference from an ideal ramp, e.g., due to a gain error of current

DAC, changes the output of the reconstructed bio-impedance.

$$\begin{aligned} T_{p_{non-L}}(m) &= \frac{1}{4f_{LF}} \\ &- \frac{\pi V_{ref}}{4\sqrt{2}f_{LF}|Z_{tissue}(m)|(I(m) \pm \Delta I(m))G_{FE}} \\ &= T_{p_L} \pm \frac{\pi V_{ref}}{4\sqrt{2}f_{LF}|Z_{tissue}(m)|I(m)G_{FE}} \times Gain_{error}. \end{aligned}$$

Based on the above equations, a gain error below 0.8% doesn't have significant effect on the reconstructed output which is a very easy goal. Also, the linearity of the front end is not the limiting factor since the required dynamic range in the pacemaker application is small.

3) *Systematic Error:* To estimate the systematic error of the system due to the semi-ramp waveform injected we use a simplified three-element heart model with a real value [18].

$$\begin{aligned} Z_{tissue} &= R_{base} + \left[R_{mem} \parallel \frac{1}{jC_{mem}\omega} \right] = \left(600 \right. \\ &\left. + \frac{70 \times 10^3}{(1 + (3.5 \times 10^{-3})^2 \omega^2)} \right) - j \frac{(3.5 \times 10^{-3})\omega}{(1 + (3.5 \times 10^{-3})^2 \omega^2)}. \end{aligned} \quad (16)$$

The quality of the semi-ramp signal and the accuracy of the comparison with the reference voltage define the systematic error of the proposed bio-impedance measurement system. The modulated input semi-ramp waveform is multiplied by the demodulation clock and subsequently filtered.

To estimate the effect of the multiplication and the effect of the low-pass filter, the first 7 harmonics of the filtered output are used. The time domain difference of the semi-ramp signal and the input filtered semi-ramp signal of the comparator is the systematic error of the system.

4) *Total Error:* To calculate the total error due to the injected signal and the system error, the amplitude and the phase of the bio-impedance are extracted from the proposed system and from the conventional lock-in amplifier bio-impedance system [10], [12], respectively.

The conventional stimulation current and demodulation clock signals are considered to be fully bi-directional square (semi-square) waves. The output of the in-phase channel modulator and quadrature channel modulator can be written as [12]:

$$\begin{aligned} V_{i.conv.}(t) &= G_{FE} I_{st} V_{clk} R_{base} + \frac{8G_{FE} I_{st} V_{clk} R_{mem}}{\pi^2} \\ &\times \left\{ \sum_{n=1}^{\infty} \left[\frac{1}{(2n-1)^2} \times \left(\frac{1}{1 + (2n-1)^2 \omega^2 R_{mem}^2 C_{mem}^2} \right) \right] \right\} \end{aligned} \quad (17)$$

$$\begin{aligned} V_{q.conv.}(t) &= \frac{8G_{FE} I_{st} V_{clk} \omega R_{mem}^2 C_{mem}}{\pi^2} \\ &\times \left\{ \sum_{n=1}^{\infty} \left[\frac{(-1)^{n+1}}{(2n-1)} \times \left(\frac{1}{1 + (2n-1)^2 \omega^2 R_{mem}^2 C_{mem}^2} \right) \right] \right\} \end{aligned} \quad (18)$$

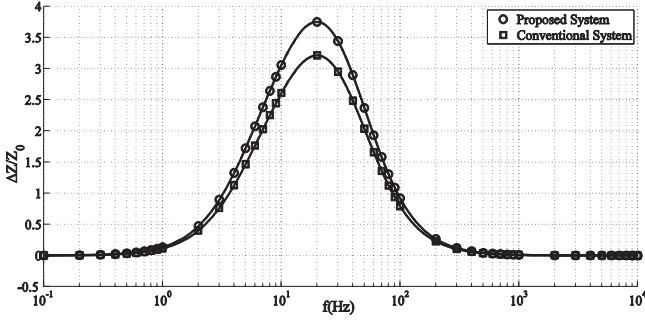


Fig. 6. Normalized amplitude error of proposed and conventional system.

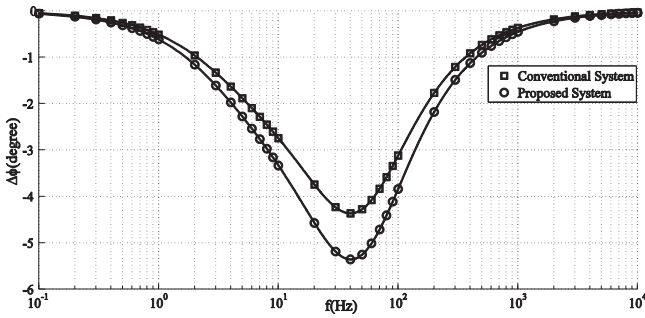


Fig. 7. Normalized phase error of proposed and conventional system.

Fig. 6 shows the total normalized amplitude error of the proposed ((12)) and the conventional system ((17) and (18)) in comparison with the theoretically correct value. Fig. 7 shows the total normalized phase error of the proposed ((13) and the conventional system ((17) and (18)) in comparison with the theoretically correct value.

C. Jitter Analysis

Jitter in the comparator affects the pulse width of the PWM output of both the magnitude and the phase channel. The pulse width relates directly to the reconstructed output signal. Thus, the jitter affects the reconstructed magnitude and phase signals. Its relation to the system parameters in the magnitude and phase channels is analyzed as follows.

1) *Magnitude-Channel Jitter Analysis*: The deviation of the pulse width in the magnitude channel is due to the jitter of the magnitude channel which originates from the electronic noise of the circuits, including that of the clock oscillator blocks. The deviation can be written from (8) as:

$$\begin{aligned}
 dT_p(m) = & -\frac{df_{LF}}{4f_{LF}^2} - \frac{\pi dV_{comp}}{4\sqrt{2}f_{LF}|Z_{tissue}|I(m)G_{FE}} \\
 & + \frac{\pi V_{comp}df_s}{4\sqrt{2}f_{LF}^2|Z_{tissue}|I(m)G_{FE}} \\
 & + \frac{\pi V_{comp}dI(m)}{4\sqrt{2}f_{LF}|Z_{tissue}|I^2(m)G_{FE}}. \quad (19)
 \end{aligned}$$

The deviation of the comparator voltage originates from the comparator input noise voltage and the noise of the front-end.

$$(dV_{comp})^2 = \sigma^2_{v_{nC}} + \sigma^2_{v_{nFE}}. \quad (20)$$

The front-end output noise can be written as:

$$\sigma^2_{v_{nFE}} = \left[\sigma^2_{i_{n,CDAC}} \times |Z_{tissue}|^2 + \sigma^2_{v_{n,irn}} \right] \times \frac{8G_{FE}^2}{\pi^2} \quad (21)$$

where $i_{n,CDAC}$ is the current noise of the current DAC and $v_{n,irn}$ is the input referred noise voltage. From (21) one can rewrite (20) as follows:

$$\begin{aligned}
 (dV_{comp})^2 = & S_{v_{nC}} B_n + \left[\sigma^2_{i_{n,CDAC}} \times |Z_{tissue}|^2 + \sigma^2_{v_{n,irn}} \right] \\
 & \times \frac{8G_{FE}^2}{\pi^2} \quad (22)
 \end{aligned}$$

where B_n is the bandwidth of the comparator and $S_{v_{nC}}$ is the power spectral density of the comparator which has a white spectrum.

As (19) shows, the variation of f_s has a direct relation with that of the output pulse width. From [17] the time deviation of the frequency (which is the jitter of the mixer clock) that originates from an oscillator is

$$\sigma^2_{f_s} = S_\varphi(f) \frac{\Delta f^2}{f_{osc}} \quad (23)$$

where Δf is the offset frequency at which the VCO phase noise of the mixer clock has been measured, $S_\varphi(f)$ is the oscillator phase noise spectrum and f_{osc} is the oscillator frequency.

Making use of (21), (22) and (23), one can rewrite (19), which is the total jitter, as:

$$\begin{aligned}
 \frac{dT_p(m)}{T_{osc}} = & \frac{\pi \sqrt{S_{v_{nC}} B_n + (\sigma^2_{i_{n,CDAC}} |Z_{tissue}|^2 + \sigma^2_{v_{n,irn}}) \times \frac{8G_{FE}^2}{\pi^2}}}{4\sqrt{2}f_{LF} |Z_{tissue}| I(m) G_{FE}} \\
 & + \frac{\sqrt{S_\varphi(f_{osc}) \frac{\Delta f^2}{f_{osc}}}}{4f_{LF}^2} + \frac{\pi V_{comp} \sqrt{S_\varphi(f_{osc}) \frac{\Delta f^2}{f_{osc}}}}{4\sqrt{2}f_{LF} |Z_{tissue}| I(m) G_{FE}} \\
 & + \frac{\pi V_{comp} \sigma_{i_{n,CDAC}}}{4\sqrt{2}f_{LF} |Z_{tissue}| I^2(m) G_{FE}}. \quad (24)
 \end{aligned}$$

The jitter caused by the channel noise is inversely proportional to the oscillator frequency (T_{osc}) while the jitter caused by the variation of the oscillator frequency has a direct square root relation. At high frequencies the jitter of the demodulation clock is the dominant factor. At lower frequencies the circuit noise including those of the comparator and the current DAC is dominant. Moreover, a higher front-end gain results in a larger effect of the current DAC noise and the input referred noise. These considerations are utilized to design a low jitter system.

2) *Phase-Channel Jitter Analysis*: The deviation of the pulse width in the phase channel originates from the front-end jitter, the inverter jitter, AND gate jitter and the jitter of the

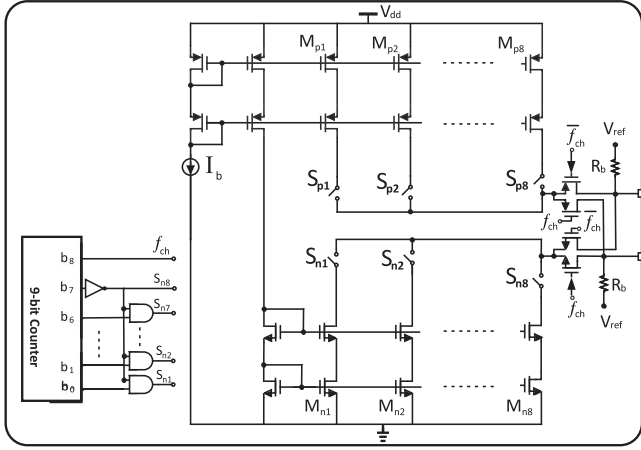


Fig. 8. Current DAC architecture and the DAC controller.

magnitude channel. Hence

$$\frac{\sigma_\tau}{T_{osc}} = \frac{\sqrt{\sigma^2_{Amp} + \sigma^2_{FE} + \sigma^2_{AND} + \sigma^2_{INV}}}{T_{osc}} \quad (25)$$

$$\sigma^2_\tau = \sigma^2_{Amp} + \sigma^2_{FE} + 3\sigma^2_{INV}$$

where we suppose that the jitter of the AND gate is twice as large as that of an inverter.

At higher frequencies, the current DAC noise, the comparator noise and the inverter noise dominate the total jitter of the phase channel, which can be decreased at the expense of higher power consumption. Based on (24) and (25) the jitter is inversely proportional to the current. Therefore, the effect of the jitter is optimized with a power-jitter trade off.

IV. CIRCUIT IMPLEMENTATION

Fig. 8 shows the 8-bit current DAC. The current DAC consists of PMOS and NMOS transistors to generate the current source and sink, respectively. The PMOS and NMOS current mirrors consist of 8-bit binary weighted sized transistors which are driven by a 4 nA precise current reference circuit. The maximum output current of the current DAC is 1 μA , which is controlled by a controller unit. An external 1 MHz oscillator is used to feed the required clock of the controller. The controller consists of an 9-bit up-counter and peripheral gates to produce the required ramp shape. The 2 kHz chopping signal, f_{ch} , is derived from the 1 MHz clock signal by means of a (divide by 512) frequency divider.

Fig. 9 shows the external circuit elements, comprising a capacitor C_b to remove the lead-heart offset, the heart tissue that is represented by the three-element model, the reference resistor (R_{sense}) for the phase channel and a high-pass filter that removes the unwanted ECG signal and any DC offset voltage. Off-chip capacitors C_b are biased with two 5 M Ω resistors at the output of the current source. Their values are chosen much greater than the tissue impedance, so that the accuracy of the bio-impedance measurement is not affected.

Fig. 10 shows the transconductance (TC) and transimpedance (TI) stages, together forming an instrumentation amplifier (IA),

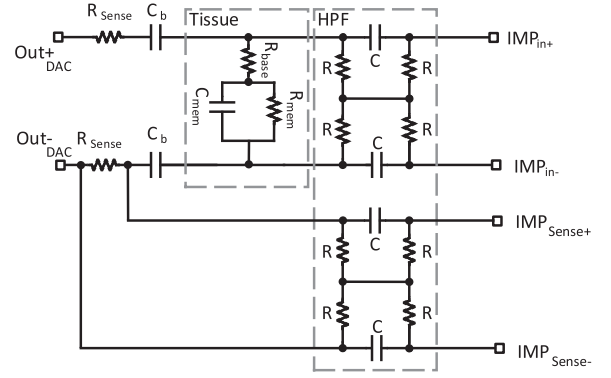
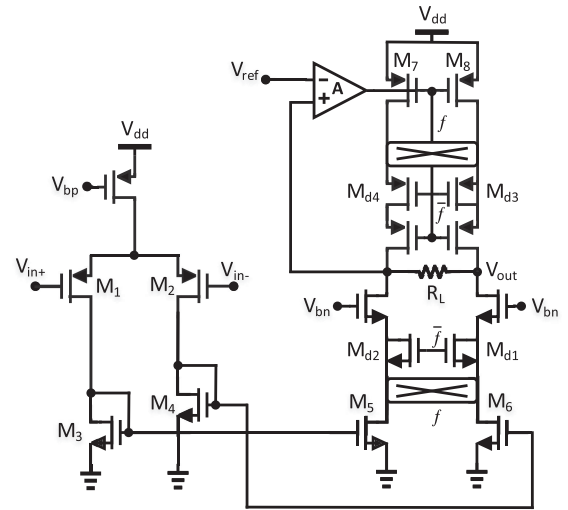
Fig. 9. Off-chip circuit components of the proposed system. It consists of the heart tissue three element model, HPF components and phase reference resistor R_{sense} .

Fig. 10. Architecture of the transconductance and transimpedance stages, together forming an instrumentation amplifier (IA), with internal mixing circuitry.

with internal mixing circuitry. The internal chopper modulator acts as a mixer to lower the output frequency. The IA benefits from dummy switches to minimize the effect of clock feed-through and charge injection. The input differential amplifier stage is followed by a current mirror and then a telescopic amplifier with its resistive output load, together providing the voltage gain (shown in Fig. 2). The input referred noise of the system can be written as:

$$\begin{aligned} \overline{V^2}_{IN} &= \frac{8kT}{g_{m1}} \left[\gamma_1 + \frac{\gamma_3 g_{m3}}{g_{m1}} + \frac{g^2_{m3}}{g_{m1} g_{m5}} (\gamma_5 + \gamma_7 \frac{g_{m7}}{g_{m5}}) \right] \\ &\quad + [4kT\gamma(g_{m1} + g_{m1} + \dots + g_{m8}) + S_{I_{bn}}] \\ &\quad \times |Z_{tissue}(\omega)|^2 \times |H_{HPF}(\omega)|^2 \\ &= \frac{8kT}{g_{m1}} \left[\gamma_1 + \frac{\gamma_3 g_{m3}}{g_{m1}} + \frac{g^2_{m3}}{g_{m1} g_{m5}} (\gamma_5 + \gamma_7 \frac{g_{m7}}{g_{m5}}) \right] \\ &\quad + 1024 (kT\gamma g_{m1} + S_{I_{bn}}) \times |Z_{tissue}(\omega)|^2 \times |H_{HPF}(\omega)|^2 \quad (26) \end{aligned}$$

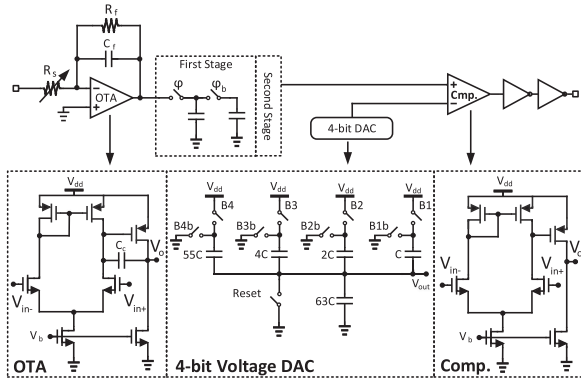


Fig. 11. Architecture of the PGA, the two-stage SC RC filter, the 4-bit voltage DAC and the comparator.

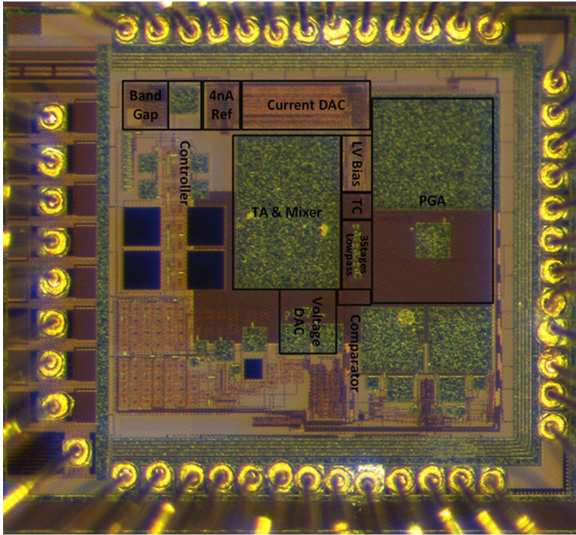


Fig. 12. Chip micrograph.

where k , γ , g_m , and S_{Ibn} denote Boltzmann's constant, the thermal noise factor, trans-conductance of the devices in Fig. 10, and the current reference noise, respectively.

Fig. 11 shows the programmable gain amplifier, the cascade of two first-order SC low-pass filters, the voltage DAC to produce the reference voltage for the comparator and finally the comparator. The PGA makes use of resistive feedback and a variable input resistor providing 4 different gain settings. The main core of the PGA is a differential input single output amplifier. The low-pass cut-off frequency of the PGA is set by a resistance and a capacitance. Cascading two stages of the 1st-order SC low-pass filter and PGA results in a -3 dB bandwidth of 900 Hz. The voltage DAC consists of 4 different capacitors. The largest capacitor provides the minimum reference voltage and the other capacitors make 8 different small voltages that are added to the minimum voltage. The comparator uses a two-stage amplifier with large input device sizes for low input offset. Two inverters provide the final outputs.

V. MEASUREMENT RESULTS

The proposed bio-impedance measurement system is fabricated in a $0.18 \mu\text{m}$ CMOS process and occupies 0.595 mm^2 .

TABLE I
DESIGN SPECIFICATION AND MEASUREMENT SUMMARY

Parameter	Target Specification	Measurement
Operating voltage	1 V	1 V
Gain	40–49–55–62 dB	39–48.5–55.5–62 dB
BW	0.5–10 Hz	0.1–10 Hz
Input Dynamic Range	3.3 mV	3.3 mV
Input referred Noise	$< 2 \mu\text{V}_{\text{rms}}$	$0.7 \mu\text{V}_{\text{rms}}$
CMRR	> 90 dB	95 dB
THD	1% @ $< 1 \text{ k}\Omega$ @ 10 Hz	1% @ $< 1 \text{ k}\Omega$ @ 10 Hz
Injection Current	0.5 – 1 μA	0.5 – 1 μA
Output Freq. Range	Up to 100 Hz	Up to 100 Hz
Tissue Impedance Range	100–3000 Ω	100–3300 Ω
Power Consumption	$< 2 \mu\text{W}$	$1.55 \mu\text{W}$

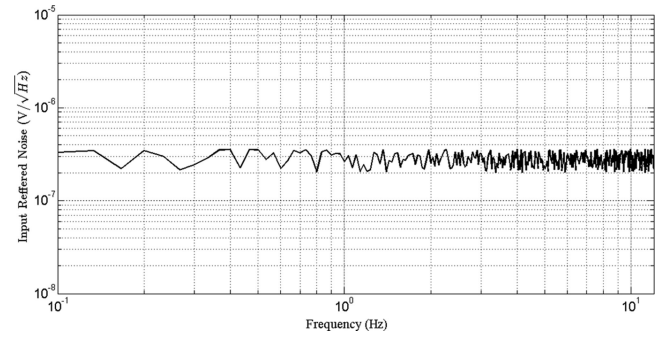


Fig. 13. Bio-impedance channel input referred noise (Gain = 40dB).

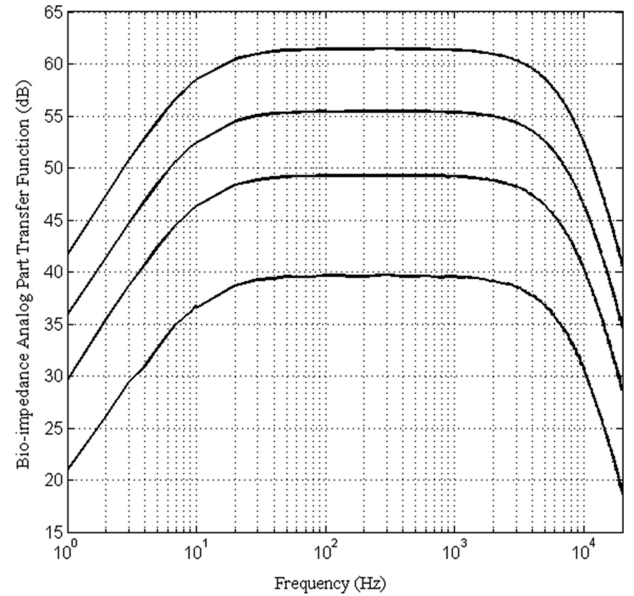


Fig. 14. Transfer functions of the PGA with its filtering characteristic.

Fig. 12 shows the chip micrograph. Table I shows the design specification summary of the system.

The input referred noise of the bio-impedance readout channel measured over a bandwidth of 0.1 Hz–10 Hz is $0.7 \mu\text{V}_{\text{rms}}$ as shown in Fig. 13 (chain gain is 40 dB) and the equivalent sensitivity of impedance measurement channel is calculated as $0.2 \Omega_{\text{rms}}/\sqrt{\text{Hz}}$ (for a total gain of 62 dB). Fig. 14 shows the

TABLE II
PERFORMANCE COMPARISON

	This Work	[10]	[11]	[19]
Technology (μ m)	0.18	0.5	0.18	0.18
Supply voltage (V)	1	2	1.8	1.2
Injection current	0.5–1 μ A	50–5.5 nA	10–40 μ A	27–117 μ A
Injection frequency	2 kHz	1 kHz	2 kHz	20 kHz
Modulation	Semi-ramp	Square	Square/Pseudo-sine	Pseudo-sine
Accuracy (Ω_{rms})	1.35	12–63	0.033–0.132	0.0098
Input referred noise*	<0.7 μ V _{rms}	1.7 μ V _{rms}	0.46 μ V _{rms}	0.612 μ V _{rms}
Bio-impedance Range (Ω)	0.1~3.3 k	0.1~10 k	0.1~4.4 k	n.a.
Overall system size (mm ²)	0.7 \times 0.85	4.6 \times 4.5	5 \times 5	3.5*1.4
Power Consumption**	1.55 μ W	6.5 μ W	50.16 μ W	58 μ W
FOM***	0.17 p	<5.5 p	0.2 p	0.29 p

*Measured over a bandwidth of 0.1–10 Hz.

** Injected current is included.

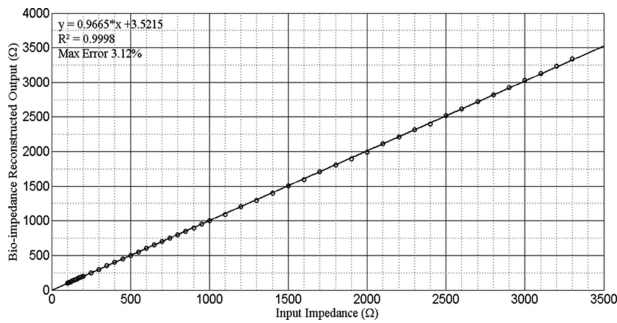
*** FOM[11] = Power/($1\Omega \times 10^{D R/20} \times f$)

Fig. 15. Characterization of the bio-impedance channel for different resistance values.

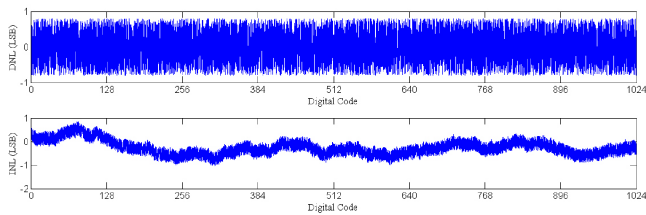


Fig. 16. Characterization of DNL and INL.

transfer function of the PGA with its filtering characteristic for four different gains (40–49–55–62 dB). To extract the system transfer characteristic (when the mixer is always on) we set the HPF corner frequency to 10 Hz while the actual frequency corner is 1 kHz in the bio-impedance measurement.

Fig. 15 shows the characterization and overall verification of the bio-impedance measurement channel for various resistances. The reconstructed output of the magnitude channel shows a linear transfer function while sweeping the measured resistance from 100 Ω to 3.3 k Ω . The maximum error equals 3.12%, which happens in the high resistance range. The high resistance range is not so important since such a high value implies lead relocation that is indicative of lead replacement. The accuracy of the bio-impedance channel is 1.35 Ω_{rms} .

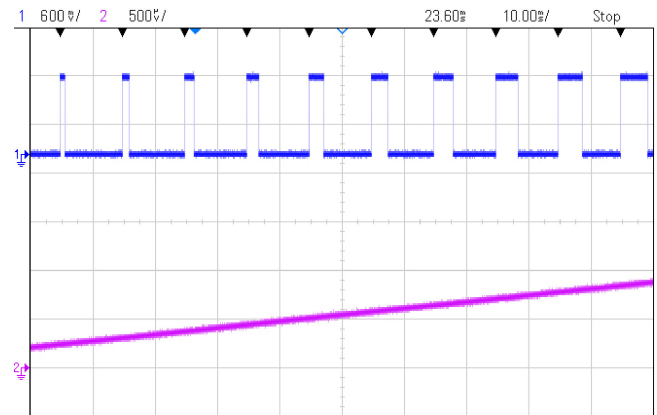


Fig. 17. Pulse width modulated output with linear increasing input (Gain = 62 dB).

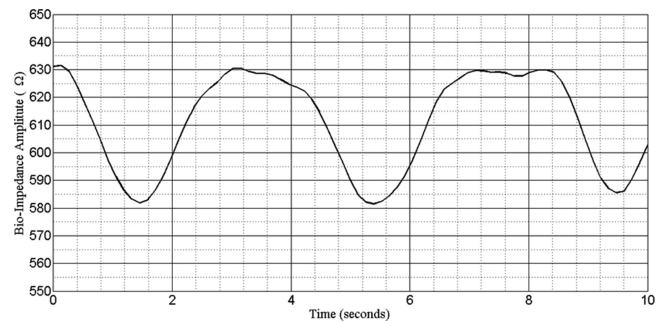


Fig. 18. Measured respiration signal on a human body using the proposed system.

After the reconstruction, the proposed system is similar to an analog to digital converter. Using the same definition of ADC parameters, we can extract the DNL and INL of the proposed system. Fig. 16 shows the DNL and INL characterization graph.

Fig. 17 shows the output pulse width modulated waveform for a linearly increasing input impedance. A higher impedance gives a higher pulse width. As the experiment was not conducted

on a real implant, the functionality of the bio-impedance measurement system is validated with respiration measured on the body as shown in Fig. 18.

Table II shows the comparison of the measurement results with those of some state-of-the-art designs. The proposed system features the lowest supply voltage and also power consumption with only $1.55 \mu\text{W}$.

VI. CONCLUSION

A $1.55 \mu\text{A}$ bio-impedance measurement IC is presented. The proposed system consists of two channels for magnitude and phase measurement, the output of which are pulse width modulated (PWM) signals. The magnitude and phase of the bio-impedance are directly related to the width of the PWM signal. The proposed system converts voltage to time and enables the transmission of its output PWM data at very low power consumption. The proposed system is capable of measuring bio-impedance signals with $1.35 \Omega_{\text{RMS}}$ accuracy.

REFERENCES

- [1] C. J. Love, *Cardiac Pacemaker and Defibrillators*, 2nd ed., Austin, TX, USA: Landes Bioscience, 2006.
- [2] J. G. Webster, *Design of Cardiac Pacemaker*, New York, NY, USA: IEEE, 1995.
- [3] S. Grimnes and Ø. G. Martinsen, *Bioimpedance and Bioelectricity Basics*, 3rd ed., San Francisco, CA, USA: Academic press, 2014.
- [4] M. Min and T. Parve, "Thoracic bioimpedance as a basis for pacing control," *Ann. New York Acad. Sci.*, vol. 873, no. 1, pp. 155–166, 1999.
- [5] M. Min and T. Parve, "Improvement of lock-in electrical bio-impedance analyzer for implantable medical devices," in *IEEE Trans. Instrum. Meas.*, vol. 56, no. 3, pp. 968–974, Jun. 2007.
- [6] P. Kassanos, L. Constantinou, I. F. Triantis, and A. Demosthenous, "An integrated analog readout for multi-frequency bioimpedance measurements," in *IEEE Sensors J.*, vol. 14, no. 8, pp. 2792–2800, Aug. 2014.
- [7] M. Min, T. Parve, A. Ronk, P. Annus, and T. Paavle, "Synchronous sampling and demodulation in an instrument for multifrequency bioimpedance measurement," in *IEEE Trans. Instrum. Meas.*, vol. 56, no. 4, pp. 1365–1372, Aug. 2007.
- [8] M. Min, T. Parve, V. Kukk, and A. Kuhlberg, "An implantable analyzer of bio-impedance dynamics: Mixed signal approach [telemetric monitors]," in *IEEE Trans. Instrum. Meas.*, vol. 51, no. 4, pp. 674–678, Aug. 2002.
- [9] M. Min, T. Parve, V. Kukk, and A. Kuhlberg, "An implantable analyzer of bio-impedance dynamics: Mixed signal approach," in *Proc. 18th IEEE Instrum. Meas. Technol. Conf.*, Budapest, 2001, vol. 1, pp. 38–43.
- [10] R. F. Yazicioglu, S. Kim, T. Torfs, H. Kim, and C. Van Hoof, "A $30 \mu\text{W}$ analog signal processor ASIC for portable biopotential signal monitoring," in *IEEE J. Solid-State Circuits*, vol. 46, no. 1, pp. 209–223, Jan. 2011.
- [11] L. Yan *et al.*, "A $13 \mu\text{A}$ analog signal processing IC for accurate recognition of multiple intra-cardiac signals," in *IEEE Trans. Biomed. Circuits Syst.*, vol. 7, no. 6, pp. 785–795, Dec. 2013.
- [12] R. Kubendran, S. Lee, S. Mitra, and R. F. Yazicioglu, "Error correction algorithm for high accuracy bio-impedance measurement in wearable healthcare applications," in *IEEE Trans. Biomed. Circuits Syst.*, vol. 8, no. 2, pp. 196–205, Apr. 2014.
- [13] L. Yan *et al.*, "A 3.9 mW 25-electrode reconfigured thoracic impedance/ECG SoC with body-channel transponder," in *Proc. IEEE Int. Solid-State Circuits Conf.*, San Francisco, CA, USA, 2010, pp. 490–491.
- [14] P. Kassanos, I. F. Triantis, and A. Demosthenous, "A CMOS magnitude/phase measurement chip for impedance spectroscopy," in *IEEE Sensors J.*, vol. 13, no. 6, pp. 2229–2236, Jun. 2013.
- [15] E. Alt, "Cardiac and pulmonary physiological analysis via intracardiac measurements with a single sensor," U.S. Patent 5.003.976, 1991.
- [16] R. A. Guinee and C. Lyden, "A novel Fourier series time function for modeling and simulation of PWM," in *IEEE Trans. Circuits Syst. I: Reg. Pap.*, vol. 52, no. 11, pp. 2427–2435, Nov. 2005.
- [17] A. A. Abidi and R. G. Meyer, "Noise in relaxation oscillators," in *IEEE J. Solid-State Circuits*, vol. 18, no. 6, pp. 794–802, Dec 1983.
- [18] S. Y. Lee *et al.*, "A programmable implantable microstimulator SoC with wireless telemetry: Application in closed-loop endocardial stimulation for cardiac pacemaker," in *IEEE Trans. Biomed. Circuits Syst.*, vol. 5, no. 6, pp. 511–522, Dec. 2011.
- [19] N. Van Helleputte *et al.*, "A $345 \mu\text{W}$ multi-sensor biomedical SoC with bio-impedance, 3-channel ECG, motion artifact reduction, and integrated DSP," in *IEEE J. Solid-State Circuits*, vol. 50, no. 1, pp. 230–244, Jan. 2015.
- [20] M. Yin and M. Ghovanloo, "Using pulse width modulation for wireless transmission of neural signals in multichannel neural recording systems," in *IEEE Trans. Neural Syst. Rehabil. Eng.*, vol. 17, no. 4, pp. 354–363, Aug. 2009.
- [21] S. Rodriguez, S. Ollmar, M. Waqar, and A. Rusu, "A batteryless sensor ASIC for implantable bio-impedance applications," in *IEEE Trans. Biomed. Circuits Syst.*, vol. 10, no. 3, pp. 533–544, Jun. 2016.
- [22] T. Master and T. Mark, "Medical electrical equipment Part 1: General requirements for basic safety and essential performance," 2012.



Milad Zamani (S'16) was born in Babol, Iran, in 1988. He received the B.Sc. degree in electrical engineering from the University of Tehran, Tehran, Iran, in 2010 and the M.Sc. degree in electrical engineering from Sharif University of Technology, Tehran, Iran, in 2012.

He is currently working toward the Ph.D. degree in the section biomedical circuit and system design at the Faculty of Electrical and Computer Engineering, University of Tehran, Tehran, Iran. His current research interests include low power analog integrated circuits and systems design for biomedical applications. He is currently a guest researcher with the Section Bioelectronics, TU Delft, Delft, The Netherlands.



Yasser Rezaeiyan was born in Khomein, Iran, in 1988. He received the B.Sc. degree in electrical engineering from Shahid Chamran University of Ahwaz, Ahwaz, Iran, in 2010 and the M.Sc. degree in electrical engineering from Sharif University of Technology, in 2012.

He is currently working towards the Ph.D. degree in the section biomedical circuit and system design in the Faculty of Electrical and Computer Engineering, University of Tehran, Tehran, Iran. His research interests include ultra-low-power analog integrated circuit and system design for biomedical applications. He is currently a guest researcher with the Section Bioelectronics, TU Delft, Delft, The Netherlands.



Omid Shoaie (M'96) received the B.Sc. and M.Sc. degrees from University of Tehran, Tehran, Iran, in 1986 and 1989, respectively, and the Ph.D. degree from Carleton University, Ottawa, ON, Canada, in 1996, all in electrical engineering.

From 1994 to 1995, he was with BNR/NORTEL, Ottawa, as a Ph.D. intern student, working on high-speed delta-sigma modulators. In 1995, he was with Philips Electronics, Inc., Ottawa, working on the design of a bandpass delta-sigma data converter.

From December 1995 to February 2000, he was a Member of Technical Staff with Bell Labs, Lucent Technologies, Allentown, PA, where he was involved in the design of mixed analog/digital integrated circuits for LAN and Fast Ethernet systems. From February 2000 to March 2003, he was with Valence Semiconductor Inc. design center in Dubai, UAE, as the Director of the mixed-signal group, where he developed voice codec and SLIC, and also several data converter IP's for 802.11a and HomePlug V.2. Later from 2004 to 2007 he developed a pair of 24-bit audio delta-sigma ADC/DAC and a 12-bit 100MHz pipeline ADC. From 2008 to 2012, he was with Qualcomm, San Diego, where he led the development of two audio codec chipsets that so far have been shipped in millions to tier one cell phone OEMs.

From 1998 to 2008, he was also an associate professor with the University of Tehran, where he has been affiliated with since Feb. 2012.

He holds 3 U.S. patents, and is the author or coauthor of more than 170 international and national journal and conference publications. His research interests include biomedical integrated circuits and systems, analog-to-digital converters, and precision analog/mixed-signal circuits and systems.



Wouter A. Serdijn (M'98–SM'08–F'11) was born in Zoetermeer ('Sweet Lake City'), the Netherlands, in 1966. He received the M.Sc. (*cum laude*) and Ph.D. degrees from Delft University of Technology, Delft, The Netherlands, in 1989 and 1994, respectively. He is currently a Full Professor in Bioelectronics at Delft University of Technology, where he heads the Section Bioelectronics, and a visiting honorary professor at the University College London, London, U.K., in the Analog and Biomedical Electronics group.

His research interests include integrated biomedical circuits and systems for biosignal conditioning and detection, neuroprosthetics, transcutaneous wireless communication, power management and energy harvesting as applied in, e.g., hearing instruments, cardiac pacemakers, cochlear implants, neurostimulators, portable, wearable, implantable and injectable medical devices and electroceuticals.

He is co-editor and co-author of the books *Analog IC Design Techniques for Nanopower Biomedical Signal Processing* (River Publishers 2016), *Design of Efficient and Safe Neural Stimulators - a multidisciplinary approach* (Springer, 2016), *EMI-Resilient Amplifier Circuits* (Springer 2013), *Ultra Low-Power Biomedical Signal Processing: an analog wavelet filter approach for pacemakers* (Springer, 2009), *Circuits and Systems for Future Generations of Wireless Communications* (Springer, 2009), *Power Aware Architecting for data dominated applications* (Springer, 2007), *Adaptive Low-Power Circuits for Wireless Communications* (Springer, 2006), *Research Perspectives on Dynamic Translinear and Log-Domain Circuits* (Kluwer, 2000), *Dynamic Translinear and Log-Domain Circuits* (Kluwer, 1998) and *Low-Voltage Low-Power Analog Integrated Circuits* (Kluwer, 1995). He authored and co-authored 8 book chapters, 2 patents and more than 300 scientific publications and presentations. He teaches Circuit Theory, Analog Integrated Circuit Design, Analog CMOS Filter Design, Active Implantable Biomedical Microsystems and Bioelectronics. He was the recipient of Electrical Engineering Best Teacher Award in 2001, in 2004 and in 2015.

He has served, a.o., the General Co-Chair for IEEE ISCAS 2015 and for IEEE BioCAS 2013, the Technical Program Chair for IEEE BioCAS 2010, and for IEEE ISCAS 2010, 2012 and 2014, as a member of the Board of Governors (BoG) of the IEEE Circuits and Systems Society (2006–2011), as the Chair of the Analog Signal Processing Technical Committee of the IEEE Circuits and Systems society, and as Editor-in-Chief for the IEEE Transactions on Circuits and Systems—I: Regular Papers (2010–2011). He is currently a member of the Steering Committee and an Associate Editor of the IEEE TRANSACTIONS ON BIOMEDICAL CIRCUITS AND SYSTEMS (T-BioCAS).

He is an IEEE Fellow, an IEEE Distinguished Lecturer and a mentor of the IEEE. In 2016, he received the IEEE Circuits and Systems Society Meritorious Service Award.